NeuroImage 297 (2024) 120706

Contents lists available at ScienceDirect

NeuroImage

journal homepage: www.elsevier.com/locate/ynimg

Memory traces of duration and location in the right intraparietal sulcus

Martin Riemer [a,b,c,*], Thomas Wolbers [c,d], Hedderik van Rijn [e]

[a] Biological Psychology and Neuroergonomics, Technical University Berlin, 10623 Berlin, Germany
[b] Bernstein Center for Computational Neuroscience (BCCN), Berlin, Germany
[c] Center for Behavioral Brain Sciences (CBBS), Magdeburg, Germany
[d] Aging, Cognition & Technology Research Group, German Center for Neurodegenerative Diseases (DZNE), Magdeburg, Germany
[e] Department of Experimental Psychology, University of Groningen, Netherlands

ARTICLE INFO

Keywords:
MVPA
fMRI
Time perception
Spatial cognition
Intraparietal sulcus
Time-space interference

ABSTRACT

Time and space form an integral part of every human experience, and for the neuronal representation of these perceptual dimensions, previous studies point to the involvement of the right-hemispheric intraparietal sulcus and structures in the medial temporal lobe. Here we used multi-voxel pattern analysis (MVPA) to investigate long-term memory traces for temporal and spatial stimulus features in those areas. Participants were trained on four images associated with short versus long durations and with left versus right locations. Our results demonstrate stable representations of both temporal and spatial information in the right posterior intraparietal sulcus. Building upon previous findings of stable neuronal codes for directly perceived durations and locations, these results show that the reactivation of long-term memory traces for temporal and spatial features can be decoded from neuronal activation patterns in the right parietal cortex.

1. Introduction

The perception of time and space is an essential aspect of every sensory experience. Every sensation occurs at a specific location and lasts for a specific duration. Many studies have been conducted to reveal the neuronal mechanisms underlying the processing of temporal and spatial information, and cross-dimensional interference effects at the behavioral level suggest at least partly overlapping neuronal networks (Bueti and Walsh, 2009; Cona et al., 2021; Gijssels et al., 2013; Lourenco and Longo, 2010; Riemer et al., 2016, 2018, 2022; Srinivasan and Carey, 2010; Walsh, 2003).

The intraparietal sulcus (IPS) in the right hemisphere and the medial temporal lobe (MTL) are plausible candidate regions for a common representation of time and space, because earlier work has demonstrated that they are involved in both temporal and spatial processing (Bueti and Walsh, 2009; Cona et al., 2021; Eichenbaum, 2017; Gijssels et al., 2013; Riemer et al., 2016; Walsh, 2003). In a recent study on the interference between travel time and traveled distance, we found that representational similarity (of time-attended and distance-attended trials) in the right IPS was correlated with the magnitude of time-space interference (Riemer et al., 2022). With respect to the MTL, animal studies have shown that both hippocampal place and entorhinal grid cells – in addition to their well-known spatially tuned firing patterns (Hafting et al., 2005; O'Keefe and Dostrovsky, 1971) – also exhibit firing patterns tuned to specific moments in time (Kraus et al., 2013, 2015). Moreover, Kraus et al. (2015) reported that a single neuron in the rodent brain can exhibit both spatially *and* temporally tuned firing patterns. There is ample evidence that the same neuronal mechanisms exist in the human brain (Deuker et al., 2016; Doeller et al., 2010; Ekstrom et al., 2003; Lee et al., 2020; Stangl et al., 2018).

Together, these findings point to the right IPS, the hippocampus and the entorhinal cortex as possible candidate regions in which information about the temporal duration and spatial location of events is stored or processed. However, studies focussing on the question as to whether those regions contain neuronal codes differentiating between the various levels of each dimension (e.g., durations of different lengths) are scarce. Hayashi et al. (2018) could show that the ability to distinguish between four different durations in the sub-second range was associated with the distinctiveness of activation patterns in the right parietal cortex, and in a recent study by Gladhill et al. (2024) is was found that the supramarginal and middle occipital gyri of the right hemisphere contained information about abstract magnitudes regarding temporal and spatial distance in a navigation task. Moreover, in these studies durations were directly presented in each trial, leaving the unresolved

* Corresponding author at: Biological Psychology and Neuroergonomics, Technical University Berlin, Fasanenstr. 1, 10623 Berlin, Germany.
E-mail address: martin.riemer@tu-berlin.de (M. Riemer).

https://doi.org/10.1016/j.neuroimage.2024.120706
Received 6 February 2024; Received in revised form 25 May 2024; Accepted 23 June 2024
Available online 25 June 2024

question whether distinctive neuronal activation patterns depend on the direct perception of durations or whether they can also be elicited on the basis of reactivated memory traces (i.e., by mere cueing of the respective duration). For the domain of time, further evidence for duration-selective coding was provided through fMRI adaptation paradigms, demonstrating increased suppression effects in the parietal cortex and the supplementary motor area for repeatedly presented durations (Hayashi et al., 2015; Protopapa et al., 2019).

With respect to the spatial domain, most evidence for location-specific neurons centers around the hippocampus (Fritch et al., 2020; Jeye et al., 2018; Shafer-Skelton and Golomb, 2016), but parietal areas are also involved in the processing of two-dimensional spatial location (Jerde et al., 2012; Lee and Baker, 2016; Sprague et al., 2014). For example, Jerde et al. (2012) used multi-voxel pattern analysis (MVPA) to decode different spatial locations displayed on a screen from the neuronal activation patterns in the posterior part of the IPS. The role of the posterior IPS in the short-term memorization of two-dimensional spatial location was confirmed by Sprague et al. (2014). Similarly, neuronal activity patterns in the hippocampus distinguish between different locations in two-dimensional space (Fritch et al., 2020; Jeye et al., 2018; Shafer-Skelton and Golomb, 2016). Another line of research provides evidence that the hexadirectional coding of three-dimensional space found in the entorhinal cortex (e.g., Doeller et al., 2010) generalizes to the representation of locations in two-dimensional visual space (Julian et al., 2018; Killian et al., 2012; Nau et al., 2018). For example, Julian et al. (2018) asked their participants to perform a visual search task on a 2D display (finding a target letter among distractor letters) and reported a sixfold modulation of the entorhinal fMRI signal as a function of gaze-movement direction. In another study, Merhav et al. (2019) found age-related deficits in spatial learning also for 2D images presented at various positions on a 2D display (instead of 3D environmental locations; Muffato et al., 2019). Together, these findings extend the role of MTL regions from three-dimensional navigation space to two-dimensional visual space.

While the role of parietal and medial temporal computations for perceptual processing and short-term retention of temporal and 2D spatial information is well established (e.g., Hayashi et al., 2018; Jerde et al., 2012; Jeye et al., 2018), the neural mechanisms underlying long-term storage and retrieval of such memory traces have received less attention. Prominent models of memory consolidation posit that the initial stages of long-term memory storage critically rely on rapid synaptic plasticity in hippocampal networks (Alvarez and Squire, 1994; Squire et al., 2015). Retrieving recently established memory traces also involves the reactivation of neocortical cell assemblies, which provide fine-grained sensory information. Over time, however, the contribution of the hippocampus may become less important, because integrated memory engrams ultimately develop in neocortical networks (Gilmore et al., 2021). Although competing models have questioned the time-limited role of the hippocampus (Sekeres et al., 2018), both viewpoints suggest that retrieving recently formed memory engrams of temporal and 2D spatial information should involve medial temporal and parietal computations.

The present study set out to test this prediction. Specifically, we hypothesized (i) that neuronal activity patterns in MTL regions and the right IPS contain both temporal and spatial information, and (ii) that these activity patterns can be triggered by mere memorization of the respective information (in contrast to direct perception), serving as long-term memory representations acquired during several learning sessions spread over two consecutive days. A positive result would reinforce the idea of duration-selective coding in these areas, as it has been proposed earlier (Hayashi et al., 2015; Hayashi and Ivry, 2020; Protopapa et al., 2019; Thavabalasingam et al., 2019), and would provide the first evidence for long-term memory traces for specific durations and 2D spatial locations. In order to ensure the reliability of our findings, two separate fMRI scanning sessions were implemented.

2. Methods

2.1. Participants

Fourteen young adults (12 males; all right-handed; mean age was 27 years, ranging from 22 to 35) participated in the study. Participants were recruited from the local community in Magdeburg and received monetary compensation. All participants gave written informed consent to the experimental protocol, which was approved by the ethics committee of the University of Magdeburg. The data of one participant were excluded from the analysis because of low quality of fMRI data (head movements, low tSNR) and poor task performance. In addition, two participants only completed the first scanning session (cf. Section 2.3.2).

2.2. Experimental stimuli

Target stimuli consisted of four fractal-like, black-and-white images (3×3 cm^2; Fig. 1A) adapted from stimuli used in Hindy et al. (2019). Each of the four fractals was orthogonally assigned to either a short or a long duration for which it was presented (1.4 or 2.9 s) and to either a left or a right location on the screen at which it was presented (8 mm left or right of the screen center). Within each participant, the coupling between fractal identity, duration, and location was kept constant throughout the entire experiment. Across participants, the assignment was quasi-randomized with the following constraint: For a set of four participants, the two fractals linked to the short duration for the first participant were linked to the left location for the second, to the long duration for the third, and to the right location for the fourth participant. More specifically, for each participant the arrangement of fractals within the coordinate system in Fig. 1A was rotated by 90 degrees.

2.3. Experimental procedure

2.3.1. Duration and location trials

In duration trials (Fig. 1C), one of the four fractals was cued for 1 s, followed by an interstimulus interval of 2 s. Then a black square frame appeared in the screen center and lasted for a variable comparison duration. After the frame offset, participants had to judge whether the cued duration was shorter (left key press) or longer (right key press) than the comparison duration.

In location trials (Fig. 1D), one of the four fractals was cued for 1 s, followed by an interstimulus interval of 2 s. Then a black square frame appeared for 2 s at a variable comparison location along the horizontal axis of the screen. After the frame offset, participants had to judge whether the cued location was left (left key press) or right (right key press) of the comparison location.

Duration and location trials were presented in separate, alternating runs. Independently for the time and the space task, comparison durations/locations were defined by means of an adaptive staircase procedure (1-up-3-down). After three consecutive correct responses, the absolute ratio between cued duration and comparison duration was reduced by 0.044 (in the time task; starting value was 1.44), or the difference between cued location and comparison location was reduced by 0.8 mm (in the space task; starting value was 8 mm). These values were chosen to ensure a comparable relation between the short/long levels in the time task and the left/right levels in the space task, as well as between the staircase step sizes in both tasks. Responses were not time-limited, and every response was directly followed by feedback (correct or false). The structure of two exemplary trials is depicted in Fig. 1C-D. At the end of each run, participants were presented with a graphical depiction of their reached performance level.

2.3.2. Training and scanning sessions

A schematic depiction of the complete experimental structure is shown in Fig. 1E. In two training sessions (one the day before, and one at the same day as MRI scanning) participants learned to associate the four

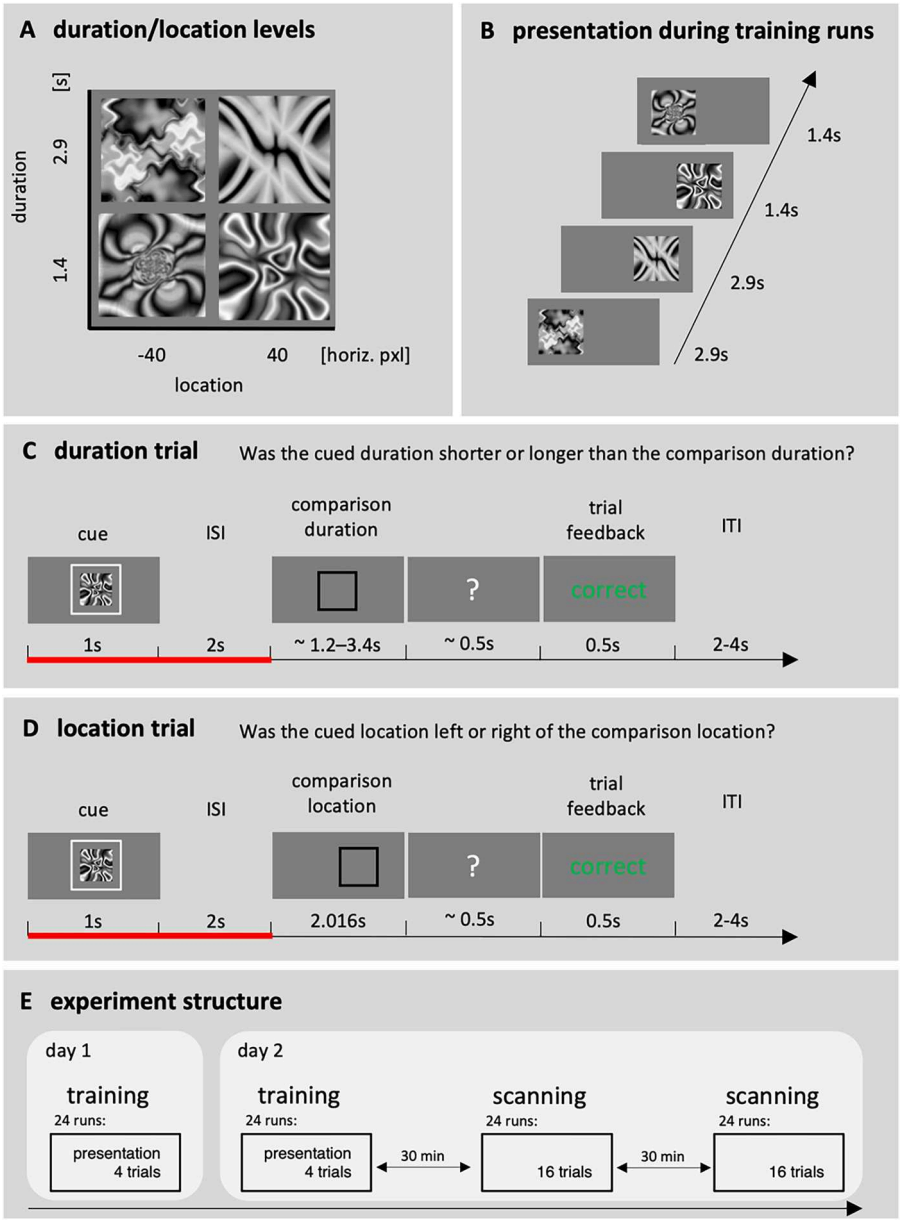

Fig. 1. Experimental stimuli and task. **(A)** Four images were assigned to a specific duration and a specific location, and **(B)** repeatedly presented during training in randomized order. **(C/D)** In the time/space task, one image was cued and a variable comparison duration/location was presented, before participants decided whether the cued image was shorter/left or longer/right than/of this comparison. Time periods used for the estimation of betas are highlighted in red. **(E)** Experimental procedure during two consecutive days. In each run of a training session, the four images were presented for/at the associated duration/location (cf. B), followed by four duration or location trials (cf. C/D). In scanning sessions, the images were not presented for/at the associated duration/location. (For interpretation of the references to color in this figure legend, the reader is referred to the web version of this article.)

fractals with their specific duration and location. Each training session consisted of 24 runs (12 duration and 12 location runs). In each training run, participants were instructed to specifically attend to either the duration or the location of the fractals. Then the fractals were sequentially presented (Fig. 1B), and directly afterwards four test trials (one for each fractal) were performed as described in Section 2.3.1. The order of fractals during presentation and test phases was randomized independently.

MRI scanning started after the second training session and was conducted in two scanning sessions, each lasting about 1.5 hours and separated by approximately thirty minutes. During these pauses, participants left the MRI scanner and took a walk on the campus. Each scanning session consisted of 24 runs (12 duration and 12 location runs)[1]. In contrast to the runs in the training sessions, each scanning run consisted of 16 trials, which were pseudo-randomized according to a de Bruijn sequence (Aguirre et al., 2011), so that each fractal was preceded once by each other fractal including itself (except, of course, for the fractal presented in the first trial, which was not preceded by the fractal

[1] For two participants, only 20 runs were performed per scanning session (10 duration and 10 location runs) due to reported feelings of unease related to lying in the scanner so long.

presented in the last trial). To refresh the participants' memories, directly at the start of each scanning session, the four fractals were presented three times (Fig. 1B), but during the rest of the session, the original durations and locations of the fractals were not shown again.

As we were interested in the neuronal activation caused by the spatiotemporal memories associated with the cue, fMRI analyses targeted the 3-second period between cue onset and comparison onset (cf. Fig. 1C-D). According to the adaptive staircase procedure (cf. Section 2.3.1), the duration/location of the comparison frame converged to the target value as the participants' performance increased. In the space task, for example, a cue associated with the right side of space would invariantly be followed by a comparison frame also at the right side. This would have been problematic, because the measured BOLD response to the cue could be affected by the congruent location of the comparison, which would interfere with our objective to induce neuronal activity patterns in the absence of direct perception. To prevent this confound, half of all trials in the scanning sessions were presented with the comparison for the respective other level (e.g., in the space task, a cue associated with the right side was followed by a comparison frame close to the uncued location on the left side). To accustom the participants to these conspicuously easy trials, the same was done for one out of four trials from the training sessions.[2]

2.4. Acquisition and preprocessing of MRI data

MRI data were acquired on a 3T Siemens Magnetom Prisma scanner, equipped with a 64-channel phased array head coil. Functional images were recorded with an echo-planar-imaging (EPI) sequence (TR = 2000 ms; TE = 25 ms; slice thickness = 1.75 mm; voxel size = 1.5 × 1.5 × 1.75 mm; number of slices = 28; field of view = 216 mm; flip angle = 80°; slice acquisition order = interleaved). Anatomical data consisted of a T1-weighted image (MPRAGE, TR = 2500 ms; TE = 2.82 ms; TI = 1100 ms; slice thickness = 1 mm; number of slices = 192; voxel size = 1 × 1 × 1 mm; field of view = 256 mm; flip angle = 7°) and a T2-weighted image (TSE, TR = 6000 ms, TE = 71 ms, slice thickness = 2 mm, number of slices = 64, voxel size = 0.5 × 0.5 × 2 mm, field of view = 224 mm, flip angle = 120°). Each session comprised 24 runs, and each run lasted about 3 minutes. Quality of fMRI data was checked with MRIQC (Esteban et al., 2017).

Functional images were preprocessed with SPM12 and Matlab R2018a v9.4.0.813654 (The MathWorks, Natick, 2018). Images were corrected for differences in slice timing, realigned to the first image collected from each subject, and smoothed using a 1 mm FWHM Gaussian filter (Hendriks et al., 2017).

Anatomical masks for early visual areas (V1/V2) and MTL regions (entorhinal cortex and hippocampus), combining both hemispheres, were created with Freesurfer v7.1.1 (Fischl, 2012), using the Desikan-Killiany atlas for segmentation of the entorhinal cortex (Desikan et al., 2006) and the automatic segmentation protocol according to Van Leemput et al. (2009) for the hippocampus. Note that only dorsal parts of the V1/V2 complex were covered by our scanning protocol (activation patterns in this region were not the primary focus of the present study and only served as a manipulation check; see Section 3.2.1). Anatomical masks for the posterior IPS were obtained as follows: The T1 image was segmented into white and gray matter images and normalized into standard MNI space. The inverse deformation field was then applied to a standard MNI space mask of the right posterior IPS (including areas hIP4-8; Richter et al., 2019) generated with the JuBrain Anatomy v3.0 SPM Toolbox Anatomy toolbox (Eickhoff et al., 2005). All masks were then coregistered to the realigned functional images. Anatomical masks for an exemplary participant are depicted in Fig. 3.

[2] This procedure also prevented a retrospective inference of the cue based on the presented comparison (i.e., it assured that it was impossible to solve the task without paying attention to the cues).

2.5. Multi-voxel pattern analysis of fMRI data

Multi-voxel pattern analysis (MVPA) was performed using the Python-based packages nilearn 0.9.2 (http://nilearn.github.io) and scikit-learn 0.21.3 (Abraham et al., 2014; Pedregosa et al., 2012). As input data, trial-wise beta estimates were calculated. For beta estimates, periods of interest covered the 3 seconds between cue onset and comparison onset (cf. Fig. 1C and D), which were modeled as delta functions that were convolved with the hemodynamic response function as implemented in SPM12. For each trial, a GLM was computed in which the specific cue was modeled as the regressor of interest. All other cues during the same run as well as all other events (and the parameters for head motion derived from spatial alignment) were modeled in separate nuisance regressors. This "LS2" approach was found to be superior in classification performance for rapid event-related designs compared to modeling each trial as a separate regressor (Mumford et al., 2012; Turner et al., 2012).

Following a region-of-interest approach, we tested the classification accuracy to differentiate between the two levels of a specific dimension (either duration or location) using either time or space runs. A logistic regression classifier was used as estimator (regularisation = l_2, C = 0.1, solver = lbfgs, scoring = roc_auc, tol = $1e^{-4}$). To prevent inflated performance estimates for the classifier due to slight data imbalances, a receiver operating characteristic (ROC) approach was implemented.

Decoding accuracies were obtained by a leave-one-run-out cross-validation. The data were split at the individual level in train and test runs and the classifier was repeatedly tested on the left-out run. Thus, there were as many folds as runs and each fold produced one accuracy value, the mean of which represents the decoding accuracy of the specific condition.

The significance of decoding accuracies were tested in R (R Core Team, 2016) by means of one-sided t-tests against chance level. For direct comparison between task types (i.e., whether participants attended to the stimuli's duration or location), classified dimensions (i.e., whether MVPA focusses on the stimuli's duration or location), and between sessions, the data were also entered into linear mixed effects models (2 × 2 × 2 factorial design) using packages *lme4* (Bates et al., 2015) and *lmerTest* (Kuznetsova et al., 2017), including the within-subjects factors *task type* (time vs. space, coded as -.5 and .5), *classified dimension* (duration vs. location, coded as -.5 and .5), and *session* (first vs. second, coded as -.5 and .5). Subjects were included as random factor.

2.6. Univariate analysis of fMRI data

For the univariate analysis, realigned functional images were normalized into standard MNI space along with the segmented T1 image (cf. Section 2.4), and then smoothed using a 4 mm FWHM Gaussian filter. Model generation and contrast estimation was done in SPM12 and Matlab R2018a v9.4.0.813654 (The MathWorks, Natick, 2018). Periods of interest covered the 3 seconds between cue onset and comparison onset (cf. Fig. 1C and D), which were modeled as delta functions that were convolved with the hemodynamic response function as implemented in SPM12. All other events as well as six head motion parameters were included as nuisance regressors. Set contrasts were *long-* versus *short-duration images* in the time task and *right-* versus *left-location images* in the space task. At the second level, two-sided one-sample t-tests were performed on these contrasts. Threshold criteria were a cluster-wise FWE ($p < .05$) and a minimum cluster size of 10 voxels.

2.7. Statistical analysis of behavioral data

For each participant, each task, and each of the four fractals (data were pooled over both sessions), psychometric functions were calculated using R package *quickpsy* (Linares and López-Moliner, 2016). Guess and lapse rates were allowed to vary between 0 and 0.2. Fitted

logistic functions represent the probability of the response 'cued duration was shorter than the comparison duration' (in the time task) or 'cued location was left of the comparison location' (in the space task), as a function of the comparison values. From the resulting functions we extracted the point of subjective equality (PSE), defined as the value of the x-axis corresponding to 50 % on the y-axis. Goodness-of-fit for the psychometric functions was calculated by deviance, ranging from 0.2 to 11.1 (Wichmann and Hill, 2001).

To enable a direct comparison between function parameters for time and space tasks, data were transformed onto a common metric before logistic functions were fitted: Comparison values (against which the cued duration/location had to be compared to) were centered (so that the value between the two levels equals 0), and rescaled (so that the lower level equals -1 and the upper level equals 1). To account for the scalar property of time perception, comparison durations were log-transformed (Wearden et al., 1997).

Data were analyzed in R (R Core Team, 2016), by fitting linear mixed effects models (2 × 2 × 2 factorial design) using packages *lme4* (Bates et al., 2015) and *lmerTest* (Kuznetsova et al., 2017), including the within-subjects factors *task type* (time vs. space, coded as -.5 and .5), *relevant dimension* (short/left vs. long/right, coded as -.5 and .5), and *irrelevant dimension* (left/short vs. right/long, coded as -.5 and .5). Subjects were included as random factor. All scripts and raw data for the analyses described in this and the previous sections can be found at OSF (https://osf.io/f2xra/).

3. Results

3.1. Behavioral results

Behavioral results are depicted in Fig. 2. The main effect of the *relevant dimension* indicates that participants could distinguish between the small and the large value of the dimension relevant for the current task (β=1.864, SE=0.057, t_{84}=32.8, $p < .001$). Although at the end of the second training session there were interindividual differences in the accuracy of temporal judgments (mean absolute ratio between cued and comparison duration was 1.18, ranging from 1.02 to 1.48) and of spatial judgments (mean difference between cued and comparison location was 2.9 mm, ranging from 0.4 to 5.6 mm), the top graphs in Fig. 2 show that every single participant memorized *short* fractals as clearly shorter than *long* fractals, and *left* fractals as more left than *right* fractals.[3]

No main effects were found for the *irrelevant dimension* (β=0.057, SE=0.057, t_{84}=1.0, $p = .32$) and *task type* (β=0.051, SE=0.057, t_{84}=0.9, $p = .37$). However, the significant interactions with *task type* indicate that the effect of the *relevant* as well as the *irrelevant dimension* was different for the time and the space task (*task type* × *relevant dimension*: β=0.233, SE=0.114, t_{84}=2.1, $p = .043$; *task type* × *irrelevant dimension*: β=-0.227, SE=0.114, t_{84}=-2.0, $p = .049$). We also found a significant 3-way interaction between *task type, relevant* and *irrelevant dimension* (β=0.469, SE=0.227, t_{84}=2.1, $p = .042$).

To investigate these interactions, we analyzed each task in a separate model. For both tasks, the separate models confirmed the effect of the *relevant dimension* (time: β=1.747, SE=0.068, t_{36}=25.6, $p < .001$; space: β=1.980, SE=0.088, t_{36}=22.5, $p < .001$). However, only for the time task we also found a significant effect of the *irrelevant dimension* (time: β=0.170, SE=0.068, t_{36}=2.5, $p = .017$; space: β=-0.056, SE=0.088, t_{36}=-0.6, $p > .5$). The interaction between the *relevant* and the *irrelevant dimension* was not significant in neither of the tasks, although a trend in the time task suggests that the effect of space on time was more pronounced for one of the two durations (time: β=-0.243, SE=0.137, t_{36}=-1.8, $p = .084$; space: β=0.226, SE=0.176, t_{36}=1.3, $p = .21$). This is in line with the significant 3-way interaction in the full model and was confirmed by subsequent t-tests showing that the short duration was judged as longer when it was associated with the right versus the left spatial side (t_{12}=3.3, $p = .003$), while the long duration was not (t_{12}=0.6, $p = .27$).

3.2. MVPA results

3.2.1. Decoding of stimulus identity in early visual areas

As a first manipulation check, we confirmed that the identity of the four visual stimuli could be decoded from activation patterns in early visual areas (V1/V2), independent of whether the task required attention to either time or space. Decoding accuracies were significantly above a chance level of 25 % (t_{12}=3.7, $p = .001$).

3.2.2. Decoding of duration and location

We compared the three regions of interest with respect to the decoding accuracies for duration and location information in the respective tasks. As depicted in Fig. 3, the right pIPS was the only region in which the fractals could be decoded, in the time task with respect to their associated duration (t_{12}=3.4, $p = .003$) and in the space task with respect to their associated location (t_{12}=2.5, $p = .014$). In MTL regions, the corresponding decoding accuracies were not significantly different from chance level, neither for the hippocampus (duration in time task: t_{12}=-0.3, $p > .5$; location in space task: t_{12}=0.5, $p = .31$) nor for the entorhinal cortex (duration in time task: t_{12}=-1.1, $p > .5$; location in space task: t_{12}=0.5, $p = .33$).

3.2.3. Decoding accuracies in right posterior IPS cannot be explained by image characteristics

To test the specificity of the decoding accuracies found in the right pIPS, we compared the accuracy values for duration in the time task and location in the space task with the accuracy values during the respective other task (e.g., decoding of duration information during the space task). These results are depicted in Fig. 4A. Duration information could be decoded above chance level during the time task (t_{12}=3.4, $p = .003$), but not during the space task (t_{12}=0.2, $p = .41$), and location information could be decoded during the space task (t_{12}=2.5, $p = .014$), but not during the time task (t_{12}=0.7, $p = .25$). Direct comparison between the decoding accuracies for both tasks (grey distributions in Fig. 4) showed that each dimension was better decoded during the corresponding task, that is, decoding accuracy for duration was higher during the time task (t_{12}=2.5, $p = .013$) and location decoding was higher during the space task (t_{12}=1.9, $p = .043$). To exclude the possibility that the performance of the decoding classifier was based on image identity rather than on the image-associated durations and locations, we performed a cross-level decoding analysis (Fig. 4C). We trained a classifier to differentiate between the two levels of the relevant dimension, but only using instances of one level of the irrelevant dimension, and then tested this classifier's performance using instances of the other level of the irrelevant dimension. For example, the classifier was trained to differentiate between left and right *short-duration* images and tested on left and right *long-duration* images. This procedure makes it impossible that the decoding accuracy is boosted by visual characteristics of the images. As depicted in Fig. 4C, duration information could still be decoded above chance level during the time task (t_{12}=2.6, $p = .011$), and location information during the space task (t_{12}=1.8, $p = .047$).

In early visual areas (V1/V2), duration and location information could also be decoded in the respective task (duration: t_{12}=3.3, $p = .003$; location: t_{12}=4.7, $p < .001$), but these above-chance decoding accuracies did not hold up to test of cross-level decoding (duration: t_{12}=0.5, $p = .31$; location: t_{12}=1.7, $p = .061$), suggesting that decoding accuracies in early visual areas are based on visual image characteristics.

The reliability of these results was confirmed by the analysis of data from a second, independent scanning session, which was identical to the first one with respect to the procedure and performed by the same

[3] Temporal and spatial accuracy were not correlated with each other (t_{11}=1.1, p=.14, r=.33), indicating that individuals with relatively high temporal accuracy did not necessarily exhibit relatively high spatial accuracy.

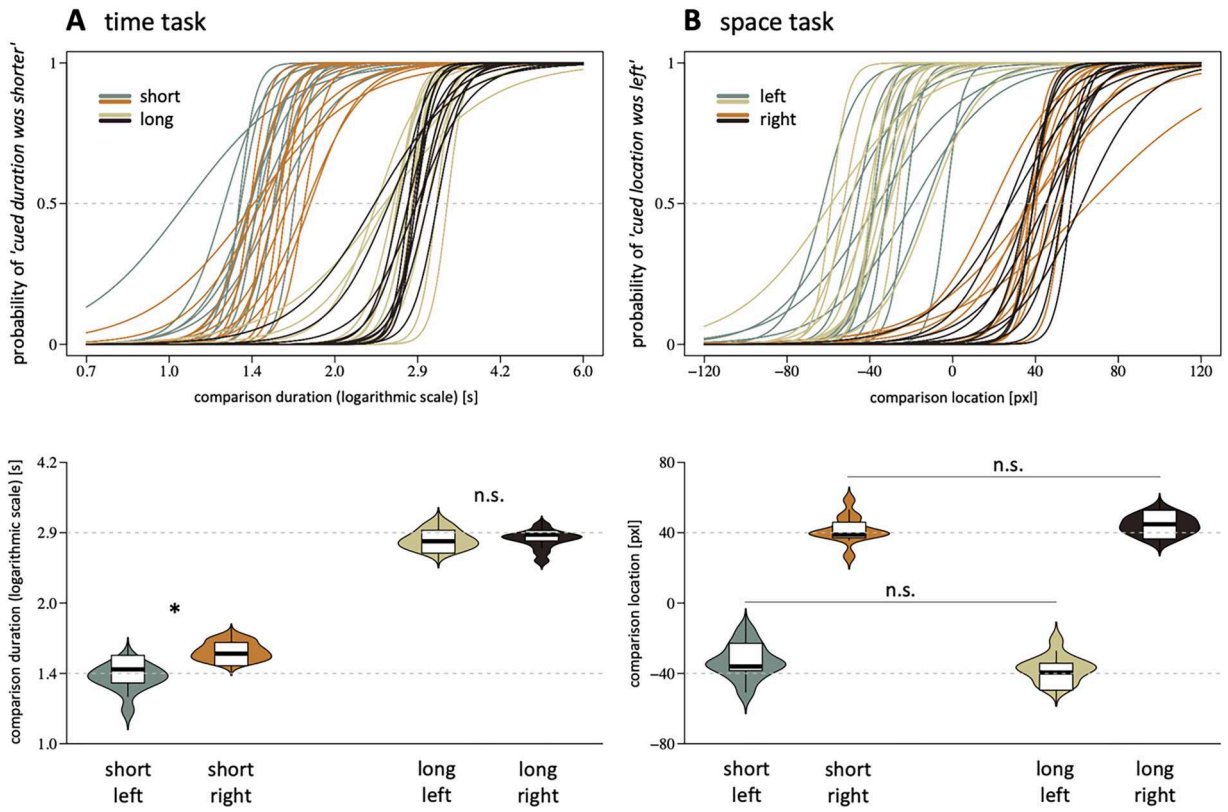

Fig. 2. Fitted logistic functions for individual subjects (top graphs) and point of subjective equality (bottom graphs) for the time task **(A)** and the space task **(B)**, depending on image category. Cross-dimensional interference was only found in the time task: The "short" image associated with the right side of space (brown) was judged as longer than the "short" image associated with the left side of space (grey). Boxplots show the median and upper/lower quartiles. (* $p < .05$; $^{n.s.}p > .05$). (For interpretation of the references to color in this figure legend, the reader is referred to the web version of this article.)

participants (except for two participants, who did not consent to a second session). As shown in Table 1 and Figs. 3 and 4, analyses of the data from the second session revealed the same pattern of results as the data from the first session, the only differences being that the decoding accuracy for location in the space task was not statistically different from that in the time task (t_{10}=1.3, p = .12), that in area V1/V2 duration information was not decodable in the time task (t_{10}=0.9, p = .20), and that in area V1/V2 cross-level decoding for location in the space task reached a significant level.

For direct comparison between sessions, task type, and classified dimensions, accuracy values were subjected to a linear mixed model. The main effect of *session* and all its interactions were not significant, indicating that the results were not statistically different between the first and the second session (session: β=0.011, SE=0.013, t_{80}=0.8, p = .40; *session* × *task type*: β=-0.004, SE=0.026, t_{76}=-0.1, $p > .5$; *session* × *classified dimension*: β=0.010, SE=0.026, t_{76}=0.4, $p > .5$; *session* × *task type* × *classified dimension*: β=-0.0005, SE=0.053, $|t_{76}|<0.1$, $p > .5$). Also the main effects of *task type* (β=-0.007, SE=0.013, t_{76}=-0.5, $p > .5$) and *classified dimension* (β=0.007, SE=0.013, t_{76}=0.5, $p > .5$) did not reach a significant level. However, there was a strong interaction between *task type* and *classified dimension* (β=0.118, SE=0.026, t_{76}=4.5, $p < .001$), indicating that duration could be decoded significantly better in the time task, whereas the decoding accuracy for location was larger in the space task.

3.2.4. Univariate fMRI results

The levels of duration/location were not consistently associated with significant differences in univariate activity. The only significant difference was found for the time task in Session 1, where *long-duration* images (in contrast to *short-duration* images) were associated with increased activity in the middle temporal gyrus of the right occipital cortex (Brodmann Area 39; MNI coordinates: 52, -66, 24; cluster size: 61 voxels; $p_{FWE\text{-}corr}$ = .001). However, this result could not be replicated in Session 2.

4. Discussion

In the present study we employed multi-voxel pattern analysis (MVPA) to test whether long-term memory traces of temporal and spatial features associated with visual stimuli can be decoded from neural activity patterns in the right intraparietal sulcus (IPS) and the medial temporal lobe (MTL). The specific regions of interest were defined on the basis of previous studies, in which it was found that both temporal and spatial processing is associated with the right IPS (Beudel et al., 2009; Bueti and Walsh, 2009; Jerde et al., 2012; Lee and Baker, 2016; Riemer et al., 2016; Sprague et al., 2014; Walsh, 2003), the hippocampus (Deuker et al., 2016; Eichenbaum, 2017; Ekstrom and Ranganath, 2018; Fritch et al., 2020; Jeye et al., 2018; Kraus et al., 2013; Shafer-Skelton and Golomb, 2016; Thavabalasingam et al., 2019), and the entorhinal cortex (Bellmund et al., 2019; Julian et al., 2018; Kraus et al., 2015; Montchal et al., 2019; Nau et al., 2018).

Our results demonstrate above-chance decoding accuracies for both temporal duration (short vs. long stimuli) and spatial location (left vs. right stimuli) in the right posterior IPS. These results provide evidence that the right parietal cortex contains information about temporal duration and spatial location, corroborating previous research on duration-selective neuronal assemblies in this area (Hayashi et al., 2015, 2018; Hayashi and Ivry, 2020; Protopapa et al., 2019). However, the present results go beyond those previous studies: Instead of being induced by direct perception, the different neuronal activity patterns in the present study were prompted by the activation of long-term memory traces regarding the temporal (or spatial) features. That is, in each trial

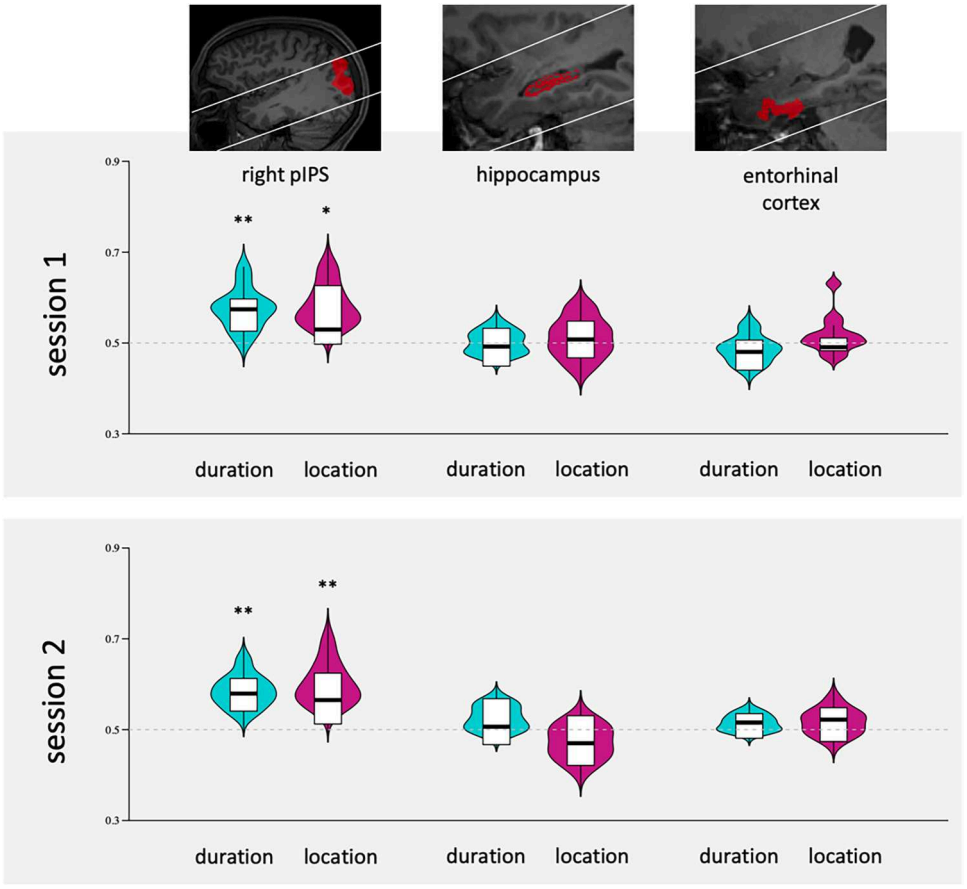

Fig. 3. Decoding accuracies for short versus long durations (turquoise) and left versus right location (violet) in the right-hemispheric posterior intraparietal sulcus (pIPS), hippocampus, and entorhinal cortex. The dashed line indicates the chance level. The area in between the two white lines in the T1 images shows the area covered by functional MRI scanning. The same pattern was found for the first and the second session. Boxplots show the median and upper/lower quartiles. (** $p <$ .01; * $p <$ .05). (For interpretation of the references to color in this figure legend, the reader is referred to the web version of this article.)

participants were presented with a stimulus *cueing* the short versus the long duration (or the left versus the right location, respectively), in contrast to being presented with the short or the long duration itself (e.g., Hayashi et al., 2018). Therefore, the present study extends previous findings in a crucial aspect: The right-hemispheric IPS not only contains information about the direct perception of *short* versus *long* durations, but it also contains a neuronal code to differentiate between long-term memories of different durations, as it has been shown for spatial location (Jerde et al., 2012; Sprague et al., 2014). These memory traces are reactivated when a certain duration (or location) is recalled or maintained in working memory (Lee and Baker, 2016).

Parietal areas are known for their role in working memory processes for spatial as well as temporal information (Curtis, 2006; Hayashi et al., 2018; Lee and Baker, 2016; Mackey and Curtis, 2017), and have been discussed as a supramodal network underlying abstract perceptual decisions (Levine and Schwarzbach, 2017). Hence, it is possible that the specific activation patterns in the right pIPS, which are associated with different levels of temporal duration and spatial location, reflect a temporary processing of reactivated memory engrams in working memory rather than the long-term memory traces themselves.

The existence of duration-selective neurons has been suggested in previous studies (Becker and Rasmussen, 2007; Hayashi et al., 2015; Hayashi and Ivry, 2020; Heron et al., 2012; Protopapa et al., 2019). For example, Hayashi et al. (2015), Hayashi and Ivry (2020) and Protopapa et al. (2019) used an adaptation paradigm and showed that repeated presentation of the same interval results in an attenuated neuronal response, primarily in parietal regions and in the supplementary motor area. This corroborates the idea of neuronal assemblies in these regions which are devoted to the processing of temporal intervals of a specific duration. This idea is further supported by psychophysical studies (Becker and Rasmussen, 2007; Heron et al., 2012; Li et al., 2017; Maarseveen et al., 2017). For example, Heron et al. (2012) found selectively increased perceptual adaptation effects when the adaptation stimuli were of a similar duration as the test stimulus. Building upon this work, the present study suggests that duration-selective neurons in the posterior part of the right IPS are also involved in the processing of reactivated memory traces for specific durations, rather than only in the direct perception of these durations.

With respect to the hippocampus and the entorhinal cortex, our data did not reveal decoding accuracies significantly above chance level, neither for temporal duration nor spatial location. Regarding temporal duration, a potential explanation for these null findings is provided by the idea that the role of MTL regions, especially of the hippocampus, for temporal processing is restricted to durations embedded within a sequence of events (Lee et al., 2020), whereas in the present study duration-associated stimuli were presented in isolation. Also regarding the decoding of spatial locations, our null finding contrasts with previous research (Hassabis et al., 2009; Shafer-Skelton and Golomb, 2016). One important difference between those and the present study is that we focussed on two-dimensional stimulus location on the screen, whereas most studies were focussed on the representation of self-location in three-dimensional space (e.g., Bonnici et al., 2012; Guo et al., 2021; Hassabis et al., 2009). However, also for the former type of stimuli, above-chance decoding accuracies have been reported (Fritch et al., 2020; Shafer-Skelton and Golomb, 2016), and Jeye et al. (2018) found that decoding accuracies for two-dimensional stimulus location were

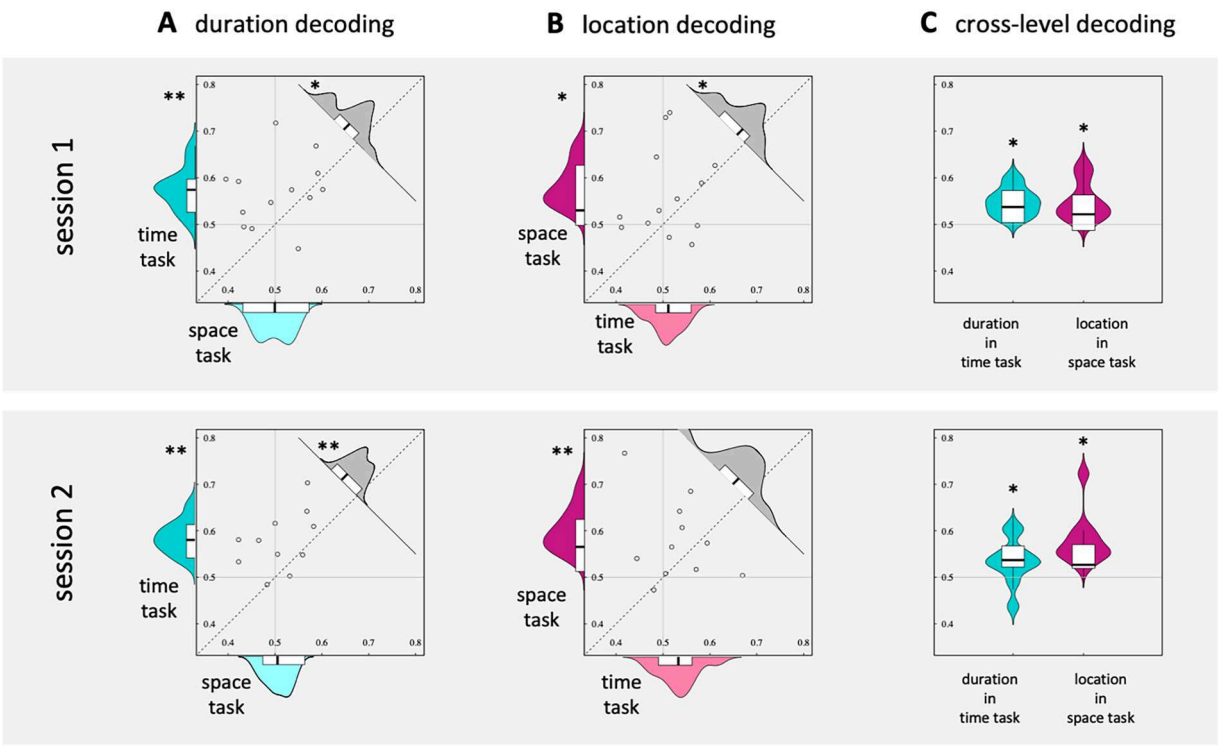

Fig. 4. Decoding accuracies in the right pIPS for two separate sessions. **(A)** Short versus long durations (turquoise) and **(B)** left versus right location (violet) were decodable from the data in the corresponding task (strong colors), but not from the data in the respective other task (light colors). Decoding accuracies for both dimensions were higher during the corresponding task compared to the respective other task (grey), except for location decoding in session 2. **(C)** Cross-level decoding for duration and location. Boxplots show the median and upper/lower quartiles. (** $p < .01$; * $p < .05$). (For interpretation of the references to color in this figure legend, the reader is referred to the web version of this article.)

Table 1
Results of decoding analyses.

Classified dimension	Brain region	Task type	Session 1		Session 2	
			t_{12}	p	t_{10}	*p*
stimulus identity	V1/V2		3.7	.001	2.6	.014
duration	HC	time	-0.3	.624	1.1	.139
	EC	time	-1.1	.857	1.0	.182
	V1/V2	time	3.3	.003	0.9	.196
		time (across levels)	0.5	.309	-0.4	.644
	right pIPS	time	3.4	.003	4.0	.001
		space	0.2	.408	0.6	.297
		time > space	2.5	.013	3.5	.003
		time (across levels)	2.6	.011	1.9	.040
location	HC	space	0.5	.314	-1.1	.849
	EC	space	0.5	.328	0.8	.227
	V1/V2	space	4.7	.001	3.0	.007
		space (across levels)	1.7	.061	1.8	.049
	right pIPS	space	2.5	.014	3.0	.007
		time	0.7	.252	1.4	.092
		space > time	1.9	.043	1.3	.116
		space (across levels)	1.8	.047	2.4	.018

correlated with measures of behavioral performance. Another possible reason for the absence of an above-chance decoding in MTL regions is the temporal signal-to-noise ratio (tSNR) of fMRI data, which was lower in the hippocampus (mean: 27.9; std: 3.0) and the entorhinal cortex (mean: 22.1; std: 3.5), compared to the posterior IPS (mean: 36.2; std: 12.3).

It is important to note that, as the present study focussed on specific regions of interest, it does not preclude the possibility of other brain regions being involved in the representation of time and space. One example is the supplementary motor area, which has been associated with the representation of time and space (Cona et al., 2021, 2023; Gladhill et al., 2024; Protopapa et al., 2019).

All significant decoding results from Session 1 were replicated in Session 2 (cf. Table 1), with one exception: Although the decoding accuracies for spatial location was above chance level in the space but not the time task, a direct comparison between these conditions revealed that the decoding accuracies for location were not statistically different in the space and the time task in Session 2 (cf. Fig. 4B). This is interesting, because the decoding accuracies for short versus long durations were always significantly higher during the time task as compared to the space task (Fig. 4A). This observation suggests that the activation of memory traces related to the spatial feature *left* versus *right location* (in contrast to the temporal feature *short* versus *long duration*) occurs more automatically, even when this specific information is irrelevant to solve the current task. This observation mirrors a finding from our previous study (Riemer et al., 2021), in which we found that the difference between the quality of retrospective and prospective judgments was smaller for spatial locations than for temporal durations. We interpreted this finding in terms of differences in the required attentional resources. While the processing of spatial information occurs almost automatically, the processing of temporal information requires deliberate attention. This interpretation is in line with the notion of higher saliency and a more holistic representation for spatial versus temporal features (Cai and Connell, 2015; Homma and Ashida, 2015; Lambrechts et al., 2013; Riemer, 2015).

Overlapping neuronal representations of temporal and spatial information in the right IPS have been proposed as a likely origin for cross-dimensional interference between time and space (Bueti and Walsh, 2009; Cona et al., 2021; Gijssels et al., 2013; Riemer et al., 2016, 2022; Walsh, 2003). However, according to the overlapping representation

hypothesis, one would expect a symmetric interference between time and space: As both dimensions resort to the same overlapping neuronal substrate, they should influence each other to the same extent. In contrast, there are numerous studies demonstrating an asymmetrical interference, with time being significantly more influenced by space than vice versa (Bottini and Casasanto, 2013; Casasanto and Boroditsky, 2008; Reali et al., 2019). The behavioral results of the present study also show that short-duration stimuli were judged as temporally longer when they were associated with the left (instead of the right) side of space, while a reversed effect of time on space could not be confirmed.

The idea of an automatic activation of spatial representations (in contrast to temporal representations) has the potential to explain the often-reported asymmetry in the interference between time and space. If the common neuronal network is more easily activated by spatial as compared to temporal information, then irrelevant spatial information should have a greater impact on perceived time than vice versa. This interpretation is supported by studies showing that the asymmetry of time-space interference can be resolved by increasing the comparability between temporal and spatial stimuli in terms of perceptual acuity (Cai et al., 2018; Cai and Connell, 2015; Cai and Wang, 2022), saliency (Homma and Ashida, 2015, 2019), or a gradual accumulation of sensory evidence (Lambrechts et al., 2013; Martin et al., 2017).

5. Conclusions

The present study provides evidence that neuronal activity patterns in the posterior part of the right IPS contain information about the temporal duration and the spatial location of memorized visual stimuli. Across two independent scanning sessions, we found stable representations of both temporal and spatial information. These results extend previous findings by demonstrating that duration-specific as well as location-specific activity patterns can be evoked by a pure memorization of the respective features (e.g., thinking about short versus long durations), rather than only by the direct perception of these stimulus features. Together, the results strengthen the idea that neuronal computations in the right IPS form the basis for cross-dimensional interference between temporal and spatial stimulus features.

Declaration of ethical approval

The study was approved by the ethics committee of the University of Magdeburg and conducted according to the ethical standards laid down in the 6th Revision of the Declaration of Helsinki (Version Seoul 2008).

Funding

This work was supported by the Deutsche Forschungsgemeinschaft (DFG, project number: 411006663), the research programme "Interval Timing in the Real World: A functional, computational and neuroscience approach", project number 453-16-005, financed by the Netherlands Organisation for Scientific Research (NWO), and the Collaborative Research in Computational Neuroscience Grant (01GQ2106) of the German Ministry of Education and Research (BMBF). None of the funding sources had direct involvement in the study.

Data and code availability statement

The datasets generated during and/or analysed during the current study are available at Open Science Framework (OSF): https://osf.io/f2xra/.

The OSF repository contains all code that was used to analyse both behavioral (https://osf.io/f2xra/behavioral/) and imaging (https://osf.io/f2xra/fmri/) data.

CRediT authorship contribution statement

Martin Riemer: Writing – original draft, Visualization, Project administration, Methodology, Investigation, Funding acquisition, Formal analysis, Conceptualization. **Thomas Wolbers:** Writing – review & editing, Resources, Methodology, Conceptualization. **Hedderik van Rijn:** Writing – review & editing, Methodology, Funding acquisition, Conceptualization.

Declaration of competing interest

The authors declare no competing financial interests.

References

Abraham, A., Pedregosa, F., Eickenberg, M., Gervais, P., Mueller, A., Kossaifi, J., Gramfort, A., Thirion, B., Varoquaux, G., 2014. Machine learning for neuroimaging with Scikit-learn. Front. Neuroinform. 8 https://doi.org/10.3389/fninf.2014.00014.

Aguirre, G.K., Mattar, M.G., Magis-Weinberg, L., 2011. De Bruijn cycles for neural decoding. Neuroimage 56 (3), 1293–1300. https://doi.org/10.1016/j.neuroimage.2011.02.005.

Alvarez, P., Squire, L.R, 1994. Memory consolidation and the medial temporal lobe: a simple network model. Proc. Natl. Acad. Sci. U.S.A. 91, 7041–7045. https://doi.org/10.1073/pnas.91.15.7041.

Bates, D., Mächler, M., Bolker, B., Walker, S., 2015. Fitting linear mixed-effects models using lme4. J. Stat. Softw. 67 (1) https://doi.org/10.18637/jss.v067.i01.

Becker, M.W., Rasmussen, I.P., 2007. The rhythm aftereffect: support for time sensitive neurons with broad overlapping tuning curves. Brain Cogn. 64 (3), 274–281. https://doi.org/10.1016/j.bandc.2007.03.009.

Bellmund, J.L., Deuker, L., Doeller, C.F., 2019. Mapping sequence structure in the human lateral entorhinal cortex. Elife 8, e45333. https://doi.org/10.7554/eLife.45333.

Beudel, M., Renken, R., Leenders, K.L., De Jong, B.M, 2009. Cerebral representations of space and time. Neuroimage 44 (3), 1032–1040. https://doi.org/10.1016/j.neuroimage.2008.09.028.

Bonnici, H.M., Kumaran, D., Chadwick, M.J., Weiskopf, N., Hassabis, D., Maguire, E.A., 2012. Decoding representations of scenes in the medial temporal lobes. Hippocampus 22 (5), 1143–1153. https://doi.org/10.1002/hipo.20960.

Bottini, R., Casasanto, D., 2013. Space and time in the child's mind: metaphoric or ATOMic? Front. Psychol. 4 https://doi.org/10.3389/fpsyg.2013.00803.

Bueti, D., Walsh, V., 2009. The parietal cortex and the representation of time, space, number and other magnitudes. Philos. Trans. R. Soc. B 364 (1525), 1831–1840. https://doi.org/10.1098/rstb.2009.0028.

Cai, Z.G., Connell, L, 2015. Space–time interdependence: evidence against asymmetric mapping between time and space. Cognition 136, 268–281. https://doi.org/10.1016/j.cognition.2014.11.039.

Cai, Z.G., Wang, R., 2022. Cross-dimensional magnitude interaction is modulated by representational noise: evidence from space–time interaction. Psychol. Res. 86 (1), 196–208. https://doi.org/10.1007/s00426-020-01472-4.

Cai, Z.G., Wang, R., Shen, M., Speekenbrink, M, 2018. Cross-dimensional magnitude interactions arise from memory interference. Cogn. Psychol. 106, 21–42. https://doi.org/10.1016/j.cogpsych.2018.08.001.

Casasanto, D., Boroditsky, L., 2008. Time in the mind: using space to think about time. Cognition 106 (2), 579–593. https://doi.org/10.1016/j.cognition.2007.03.004.

Cona, G., Wiener, M., Scarpazza, C., 2021. From ATOM to GradiATOM: cortical gradients support time and space processing as revealed by a meta-analysis of neuroimaging studies. Neuroimage 224, 117407. https://doi.org/10.1016/j.neuroimage.2020.117407.

Cona, G., Wiener, M., Allegrini, F., Scarpazza, C, 2023. Gradient organization of space, time, and numbers in the brain: a meta-analysis of neuroimaging studies. Neuropsychol. Rev. https://doi.org/10.1007/s11065-023-09609-z.

Curtis, C.E., 2006. Prefrontal and parietal contributions to spatial working memory. Neuroscience 139, 173–180. https://doi.org/10.1016/j.neuroscience.2005.04.070.

Desikan, R.S., Ségonne, F., Fischl, B., Quinn, B.T., Dickerson, B.C., Blacker, D., Buckner, R.L., Dale, A.M., Maguire, R.P., Hyman, B.T., Albert, M.S., Killiany, R.J., 2006. An automated labeling system for subdividing the human cerebral cortex on MRI scans into gyral based regions of interest. Neuroimage 31 (3), 968–980. https://doi.org/10.1016/j.neuroimage.2006.01.021.

Deuker, L., Bellmund, J.L., Navarro Schröder, T., Doeller, C.F., 2016. An event map of memory space in the hippocampus. Elife 5, e16534. https://doi.org/10.7554/eLife.16534.

Doeller, C.F., Barry, C., Burgess, N., 2010. Evidence for grid cells in a human memory network. Nature 463 (7281), 657–661. https://doi.org/10.1038/nature08704.

Eichenbaum, H., 2017. Time (and space) in the hippocampus. Curr. Opin. Behav. Sci. 17, 65–70. https://doi.org/10.1016/j.cobeha.2017.06.010.

Eickhoff, S.B., Stephan, K.E., Mohlberg, H., Grefkes, C., Fink, G.R., Amunts, K., Zilles, K., 2005. A new SPM toolbox for combining probabilistic cytoarchitectonic maps and functional imaging data. Neuroimage 25 (4), 1325–1335. https://doi.org/10.1016/j.neuroimage.2004.12.034.

Ekstrom, A.D., Kahana, M.J., Caplan, J.B., Fields, T.A., Isham, E.A., Newman, E.L., Fried, I., 2003. Cellular networks underlying human spatial navigation. Nature 425 (6954), 184–188. https://doi.org/10.1038/nature01964.

Ekstrom, A.D., Ranganath, C., 2018. Space, time, and episodic memory: the hippocampus is all over the cognitive map. Hippocampus 28 (9), 680–687. https://doi.org/10.1002/hipo.22750.
Esteban, O., Birman, D., Schaer, M., Koyejo, O.O., Poldrack, R.A., Gorgolewski, K.J., 2017. MRIQC: advancing the automatic prediction of image quality in MRI from unseen sites. PLoS. One 12 (9), e0184661. https://doi.org/10.1371/journal.pone.0184661.
Fischl, B., 2012. FreeSurfer. Neuroimage 62 (2), 774–781. https://doi.org/10.1016/j.neuroimage.2012.01.021.
Fritch, H.A., MacEvoy, S.P., Thakral, P.P., Jeye, B.M., Ross, R.S., Slotnick, S.D., 2020. The anterior hippocampus is associated with spatial memory encoding. Brain Res. 1732, 146696 https://doi.org/10.1016/j.brainres.2020.146696.
Gijssels, T., Bottini, R., Rueschemeyer, S.-A., Casasanto, D., 2013. Space and time in the parietal cortex: fMRI Evidence for a neural asymmetry. In: Proceedings of the 35th Annual Meeting of the Cognitive Science Society (CogSci 2013). Cognitive Science Society, pp. 495–500. http://mindmodeling.org/cogsci2013/papers/0113/index.html.
Gilmore, A.W., Quach, A., Kalinowski, S.E., González-Araya, E.I., Gotts, S.J., Schacter, D. L., Martin, A., 2021. Evidence supporting a time-limited hippocampal role in retrieving autobiographical memories. Proc. Natl. Acad. Sci. U.S.A. 118 (12), e2023069118 https://doi.org/10.1073/pnas.2023069118.
Gladhill, K.A., Robinson, E.M., Stanfield-Wiswell, C., Bader, F., Wiener, M., 2024. Separable representations for duration and distance in virtual movements. J. Cogn. Neurosci. 36 (3), 447–459. https://doi.org/10.1162/jocn_a_02097.
Guo, J., Zhang, K., Zhang, J., Zhao, R., Liang, Y., Lin, Y., Yu, S., Qin, W., Yang, X., 2021. Decoding spatial memory retrieval in cubical space using fMRI signals. Front. Neural Circ. 15, 624352 https://doi.org/10.3389/fncir.2021.624352.
Hafting, T., Fyhn, M., Molden, S., Moser, M.-B., Moser, E.I., 2005. Microstructure of a spatial map in the entorhinal cortex. Nature 436 (7052), 801–806. https://doi.org/10.1038/nature03721.
Hassabis, D., Chu, C., Rees, G., Weiskopf, N., Molyneux, P.D., Maguire, E.A., 2009. Decoding neuronal ensembles in the human hippocampus. Curr. Biol. 19 (7), 546–554. https://doi.org/10.1016/j.cub.2009.02.033.
Hayashi, M.J., Ditye, T., Harada, T., Hashiguchi, M., Sadato, N., Carlson, S., Walsh, V., Kanai, R, 2015. Time adaptation shows duration selectivity in the human parietal cortex. PLoS. Biol. 13 (9), e1002262 https://doi.org/10.1371/journal.pbio.1002262.
Hayashi, M.J., Ivry, R.B., 2020. Duration selectivity in right parietal cortex reflects the subjective experience of time. J. Neurosci. 40 (40), 7749–7758. https://doi.org/10.1523/JNEUROSCI.0078-20.2020.
Hayashi, M.J., Van Der Zwaag, W., Bueti, D., Kanai, R., 2018. Representations of time in human frontoparietal cortex. Commun. Biol. 1 (1), 233. https://doi.org/10.1038/s42003-018-0243-z.
Hendriks, M.H.A., Daniels, N., Pegado, F., Op De Beeck, H.P., 2017. The effect of spatial smoothing on representational similarity in a simple motor paradigm. Front. Neurol. 8, 222. https://doi.org/10.3389/fneur.2017.00222.
Heron, J., Aaen-Stockdale, C., Hotchkiss, J., Roach, N.W., McGraw, P.V., Whitaker, D., 2012. Duration channels mediate human time perception. Proc. R. Soc. B 279 (1729), 690–698. https://doi.org/10.1098/rspb.2011.1131.
Hindy, N.C., Avery, E.W., Turk-Browne, N.B., 2019. Hippocampal-neocortical interactions sharpen over time for predictive actions. Nat. Commun. 10 (1), 3989. https://doi.org/10.1038/s41467-019-12016-9.
Homma, C.T., Ashida, H., 2015. What makes space-time interactions in human vision asymmetrical? Front. Psychol. 6 https://doi.org/10.3389/fpsyg.2015.00756.
Homma, C.T., Ashida, H., 2019. Temporal cognition can affect spatial cognition more than vice versa: the effect of task-related stimulus saliency. Multisens. Res. 32 (1), 25–44. https://doi.org/10.1163/22134808-20181287.
Jerde, T.A., Merriam, E.P., Riggall, A.C., Hedges, J.H., Curtis, C.E., 2012. Prioritized maps of space in human frontoparietal cortex. J. Neurosci. 32 (48), 17382–17390. https://doi.org/10.1523/JNEUROSCI.3810-12.2012.
Jeye, B.M., MacEvoy, S.P., Karanian, J.M., Slotnick, S.D., 2018. Distinct regions of the hippocampus are associated with memory for different spatial locations. Brain Res. 1687, 41–49. https://doi.org/10.1016/j.brainres.2018.02.029.
Julian, J.B., Keinath, A.T., Frazzetta, G., Epstein, R.A, 2018. Human entorhinal cortex represents visual space using a boundary-anchored grid. Nat. Neurosci. 21 (2), 191–194. https://doi.org/10.1038/s41593-017-0049-1.
Killian, N.J., Jutras, M.J., Buffalo, E.A., 2012. A map of visual space in the primate entorhinal cortex. Nature 491 (7426), 761–764. https://doi.org/10.1038/nature11587.
Kraus, B.J., Brandon, M.P., Robinson, R.J., Connerney, M.A., Hasselmo, M.E., Eichenbaum, H., 2015. During running in place, grid cells integrate elapsed time and distance run. Neuron 88 (3), 578–589. https://doi.org/10.1016/j.neuron.2015.09.031.
Kraus, B.J., Robinson, R.J., White, J.A., Eichenbaum, H., Hasselmo, M.E., 2013. Hippocampal "time cells": time versus path integration. Neuron 78 (6), 1090–1101. https://doi.org/10.1016/j.neuron.2013.04.015.
Kuznetsova, A., Brockhoff, P.B., Christensen, R.H.B., 2017. lmerTest Package: tests in linear mixed effects models. J. Stat. Softw. 82 (13) https://doi.org/10.18637/jss.v082.i13.
Lambrechts, A., Walsh, V., van Wassenhove, V, 2013. Evidence accumulation in the magnitude system. PLoS ONE 8 (12), e82122. https://doi.org/10.1371/journal.pone.0082122.
Lee, S.-H., Baker, C.I., 2016. Multi-voxel decoding and the topography of maintained information during visual working memory. Front. Syst. Neurosci. 10 https://doi.org/10.3389/fnsys.2016.00002.
Lee, A.C.H., Thavabalasingam, S., Alushaj, D., Çavdaroğlu, B., Ito, R., 2020. The hippocampus contributes to temporal duration memory in the context of event sequences: a cross-species perspective. Neuropsychologia 137, 107300. https://doi.org/10.1016/j.neuropsychologia.2019.107300.
Levine, S.M., Schwarzbach, J., 2017. Decoding of auditory and tactile perceptual decisions in parietal cortex. Neuroimage 162, 297–305. https://doi.org/10.1016/j.neuroimage.2017.08.060.
Li, B., Xiao, L., Yin, H., Liu, P., Huang, X., 2017. Duration aftereffect depends on the duration of adaptation. Front. Psychol. 8 https://doi.org/10.3389/fpsyg.2017.00491.
Linares, D., López-Moliner, J, 2016. quickpsy: an R package to fit psychometric functions for multiple groups. R. J. 8 (1), 122. https://doi.org/10.32614/RJ-2016-008.
Lourenco, S.F., Longo, M.R., 2010. General magnitude representation in human infants. Psychol. Sci. 21 (6), 873–881. https://doi.org/10.1177/0956797610370158.
Maarseveen, J., Hogendoorn, H., Verstraten, F.A.J., Paffen, C.L.E., 2017. An investigation of the spatial selectivity of the duration after-effect. Vision. Res. 130, 67–75. https://doi.org/10.1016/j.visres.2016.11.003.
Mackey, W.E., Curtis, C.E., 2017. Distinct contributions by frontal and parietal cortces support working memory. Sci. Rep. 7, 6188. https://doi.org/10.1038/s41598-017-06293-x.
Martin, B., Wiener, M., van Wassenhove, V., 2017. A Bayesian perspective on accumulation in the magnitude system. Sci. Rep. 7 (1), 630. https://doi.org/10.1038/s41598-017-00680-0.
Merhav, M., Riemer, M., Wolbers, T., 2019. Spatial updating deficits in human aging are associated with traces of former memory representations. Neurobiol. Aging 76, 53–61. https://doi.org/10.1016/j.neurobiolaging.2018.12.010.
Montchal, M.E., Reagh, Z.M., Yassa, M.A., 2019. Precise temporal memories are supported by the lateral entorhinal cortex in humans. Nat. Neurosci. 22 (2), 284–288. https://doi.org/10.1038/s41593-018-0303-1.
Muffato, V., Hilton, C., Meneghetti, C., De Beni, R., Wiener, J.M., 2019. Evidence for age-related deficits in object-location binding during place recognition. Hippocampus 29 (10), 971–979. https://doi.org/10.1002/hipo.23099.
Mumford, J.A., Turner, B.O., Ashby, F.G., Poldrack, R.A., 2012. Deconvolving BOLD activation in event-related designs for multivoxel pattern classification analyses. Neuroimage 59 (3), 2636–2643. https://doi.org/10.1016/j.neuroimage.2011.08.076.
Nau, M., Navarro Schröder, T., Bellmund, J.L.S., Doeller, C.F., 2018. Hexadirectional coding of visual space in human entorhinal cortex. Nat. Neurosci. 21 (2), 188–190. https://doi.org/10.1038/s41593-017-0050-8.
O'Keefe, J., Dostrovsky, J., 1971. The hippocampus as a spatial map. Preliminary evidence from unit activity in the freely-moving rat. Brain Res. 34 (1), 171–175. https://doi.org/10.1016/0006-8993(71)90358-1.
Pedregosa, F., Varoquaux, G., Gramfort, A., Michel, V., Thirion, B., Grisel, O., Blondel, M., Müller, A., Nothman, J., Louppe, G., Prettenhofer, P., Weiss, R., Dubourg, V., Vanderplas, J., Passos, A., Cournapeau, D., Brucher, M., Perrot, M., Duchesnay, É., 2012. Scikit-learn: Machine Learning in Python. https://doi.org/10.48550/ARXIV.1201.0490.
Protopapa, F., Hayashi, M.J., Kulashekhar, S., Van Der Zwaag, W., Battistella, G., Murray, M.M., Kanai, R., Bueti, D., 2019. Chronotopic maps in human supplementary motor area. PLoS Biol. 17 (3), e3000026 https://doi.org/10.1371/journal.pbio.3000026.
R Core Team, 2016. R: A Language and Environment for Statistical Computing. R Foundation for Statistical Computing, Vienna, Austria.
Reali, F., Lleras, M., Alviar, C., 2019. Asymmetrical time and space interference in Tau and Kappa effects. Cogent. Psychol. 6 (1), 1568069 https://doi.org/10.1080/23311908.2019.1568069.
Richter, M., Amunts, K., Mohlberg, H., Bludau, S., Eickhoff, S.B., Zilles, K., Caspers, S., 2019. Cytoarchitectonic segregation of human posterior intraparietal and adjacent parieto-occipital sulcus and its relation to visuomotor and cognitive functions. Cereb. Cortex 29 (3), 1305–1327. https://doi.org/10.1093/cercor/bhy245.
Riemer, M., 2015. Psychophysics and the anisotropy of time. Conscious. Cogn. 38, 191–197. https://doi.org/10.1016/j.concog.2015.06.007.
Riemer, M., Achtzehn, J., Kuehn, E., Wolbers, T., 2022. Cross-dimensional interference between time and distance during spatial navigation is mediated by speed representations in intraparietal sulcus and area hMT+. Neuroimage 257, 119336. https://doi.org/10.1016/j.neuroimage.2022.119336.
Riemer, M., Diersch, N., Bublatzky, F., Wolbers, T., 2016. Space, time, and numbers in the right posterior parietal cortex: Differences between response code associations and congruency effects. Neuroimage 129, 72–79. https://doi.org/10.1016/j.neuroimage.2016.01.030.
Riemer, M., Shine, J.P., Wolbers, T., 2018. On the (a)symmetry between the perception of time and space in large-scale environments. Hippocampus 28 (8), 539–548. https://doi.org/10.1002/hipo.22954.
Riemer, M., Wolbers, T., van Rijn, H, 2021. Age-related changes in time perception: the impact of naturalistic environments and retrospective judgements on timing performance. Quart. J. Exp. Psychol. 74 (11), 2002–2012. https://doi.org/10.1177/17470218211023362.
Sekeres, M.J., Winocur, G., Moscovitch, M., 2018. The hippocampus and related neocortical structures in memory transformation. Neurosci. Lett. 680, 39–53. https://doi.org/10.1016/j.neulet.2018.05.006.
Shafer-Skelton, A., Golomb, J., 2016. Decoding of visual stimulus location in the human hippocampus. J. Vis. 16 (12), 873. https://doi.org/10.1167/16.12.873.
Sprague, T.C., Ester, E.F., Serences, J.T., 2014. Reconstructions of information in visual spatial working memory degrade with memory load. Curr. Biol. 24 (18), 2174–2180. https://doi.org/10.1016/j.cub.2014.07.066.

Squire, L.R., Genzel, L., Wixted, J.T., Morris, R.G., 2015. Memory Consolidation. Cold. Spring. Harb. Perspect. Biol. 7, a021766. https://cshperspectives.cshlp.org/content/7/8/a021766.

Srinivasan, M., Carey, S., 2010. The long and the short of it: on the nature and origin of functional overlap between representations of space and time. Cognition 116 (2), 217–241. https://doi.org/10.1016/j.cognition.2010.05.005.

Stangl, M., Achtzehn, J., Huber, K., Dietrich, C., Tempelmann, C., Wolbers, T., 2018. Compromised grid-cell-like representations in old age as a key mechanism to explain age-related navigational deficits. Curr. Biol. 28 (7), 1108–1115. https://doi.org/10.1016/j.cub.2018.02.038.

Thavabalasingam, S., O'Neil, E.B., Tay, J., Nestor, A., Lee, A.C.H., 2019. Evidence for the incorporation of temporal duration information in human hippocampal long-term memory sequence representations. Proc. Natl. Acad. Sci. 116 (13), 6407–6414. https://doi.org/10.1073/pnas.1819993116.

Turner, B.O., Mumford, J.A., Poldrack, R.A., Ashby, F.G., 2012. Spatiotemporal activity estimation for multivoxel pattern analysis with rapid event-related designs. Neuroimage 62 (3), 1429–1438. https://doi.org/10.1016/j.neuroimage.2012.05.057.

Van Leemput, K., Bakkour, A., Benner, T., Wiggins, G., Wald, L.L., Augustinack, J., Dickerson, B.C., Golland, P., Fischl, B., 2009. Automated segmentation of hippocampal subfields from ultra-high resolution in vivo MRI. Hippocampus 19 (6), 549–557. https://doi.org/10.1002/hipo.20615.

Walsh, V., 2003. A theory of magnitude: Common cortical metrics of time, space and quantity. Trends. Cogn. Sci. 7 (11), 483–488. https://doi.org/10.1016/j.tics.2003.09.002.

Wearden, J.H., Denovan, L., Haworth, R., 1997. Scalar timing in temporal generalization in humans with longer stimulus durations. J. Exp. Psychol. 23 (4), 502–511. https://doi.org/10.1037/0097-7403.23.4.502.

Wichmann, F.A., Hill, N.J., 2001. The psychometric function: I. Fitting, sampling, and goodness of fit. Percept. Psychophys. 63 (8), 1293–1313. https://doi.org/10.3758/BF03194544.